3D GEOLOGIC VIRTUAL MODELING: SMARTPHONE-BASED REMOTE SENSING FOR SURVEYING AND VISUALIZING A SECTION OF LA INDEPENDENCIA MINE, COLOMBIA

A RESEARCH PAPER PRESENTED TO
THE DEPARTMENT OF HUMANITIES AND SOCIAL SCIENCES
IN CANDIDACY FOR THE DEGREE OF
MASTER OF SCIENCE

By
MANUEL A. ACOSTA

NORTHWEST MISSOURI STATE UNIVERSITY
MARYVILLE, MISSOURI
DECEMBER, 2024

1. Introduction

In recent years, there has been a growing interest in utilizing advanced technologies and digital tools to increase geological science research, education, and application. With the continuous improvement of three-dimensional (3D) visualization, virtual reality (VR), and remote sensing techniques, geology has witnessed significant advancements in mapping, modeling, and creating virtual models. These developments have opened new possibilities to explore and understand geological scenes in an immersive and efficient manner.

One area of research focuses on the development of geologic 3D models, also referred to as digital outcrop models (DOM´s) (Burton et al., 2011; Tavani et al., 2022), using remote sensing techniques. These virtual models aim to provide an alternative and complement to traditional geologic mapping and surveying. The creation of accurate 3D digital models of geologic formations such as outcrops and underground exposures can be addressed through the use of Light Detection and Ranging (LiDAR) (Di Stefano et al., 2021, Huber and Vandapel 2006) and photogrammetry (Janiszewski et al., 2022) techniques. Geologic virtual 3D models have the potential to automate mapping processes (Janiszewski et al., 2022; Sampaio et al., 2023), to enhance the visualization of objects and their geometrical relationships (Błaszczak-Bąk et al., 2023), and, to facilitate lithological differentiation to distinguish between different rock types (Burton et al., 2011; Penasa et al., 2014; Humair et al., 2015). Performing 3D reconstructions in underground environments is not an easy task due to the lack of adequate lighting, homogeneity of color and shape of the objects to be measured, as well as the presence of dust in the air (Abbas and Abed 2024; Świerczyńska et al., 2024).

Due to constraints in technology and software, point cloud data obtained through traditional remote sensors has mostly been collected and used by professional personnel and

equipment. Today, it is possible for common users to gain access to reality capture capabilities. The use of iPhones as remote sensing tools is a recent technology that started in 2020 when the LiDAR-enabled iPad Pro and iPhone 12 Pro were released to the market (Abbas and Abed 2024), contrasting with the introduction of terrestrial laser scanning (TLS) (1990s) and mobile laser scanning (MLS) (2000s) (Askar and Sternberg 2023). Apple's models have been at the forefront of adopting LiDAR technology combined with powerful cameras, enabling enhanced photography, videography, and augmented reality (AR) experiences. With the ability to capture detailed scans and measurements on the go, users can now easily create detailed models with just their smartphone. Several methods and applications (apps) are available for collecting and processing 3D point clouds. The choice of the right method depends on factors such as the type of application, costs, time, accuracy, and efficiency. The AR kit (ARKit) integrated into iPhones facilitates the acquisition of scans during photogrammetric image processing, whether utilizing the smartphone's camera or through direct measurements obtained via the iPhone's LiDAR sensor (Askar and Sternberg 2023; Sampaio et al., 2023; Świerczyńska et al., 2024).

While these technological advancements have shown promise, there are still challenges to address. Accuracy and reliability in the restitution and segmentation of 3D models, and the implementation of open-source tools for visualization and analysis (software) as well as affordable alternatives for the creation of the geological models (hardware) are areas that can benefit from further research and development.

1.1 Research Objective

The objective of this research is to use affordable and open-source tools to create and visualize geologic virtual 3D models of a section of an underground mine located in Titiribí, Colombia. The study aims to contribute to developing a practical way for implementing LiDAR

and photogrammetry smartphone-based remote sensing techniques in this type of underground environment. The research also presents the following secondary objectives: 1) Conducting accuracy assessments by comparing point cloud densities and performing in-situ manual measurements to verify the accuracy and precision of the LiDAR and Photogrammetry methods used to create the 3D models. 2) Segmenting a 3D point cloud to detect lithological changes using LiDAR intensity values. 3) Integrating a 3D inverse distance weighting (IDW) interpolation of quartz vein grade values with one of the 3D models to enhance geological characterization and visual interpretation of this part of the deposit.

Smartphone-based remote sensing represents a recent advancement, which accounts for the relatively limited number of studies published to date. The application of smartphones to capture 3D point clouds in underground spaces and utilize their LiDAR sensors to record intensity values for enhancing underground geology mapping is particularly underexplored. Although traditional methods such as TLS have been employed extensively for mapping rock formations, there is a scarcity of research utilizing smartphones for these purposes. Existing research has been conducted within mining, geotechnical and risk management contexts, with minimal exploration of smartphones' potential for lithological mapping or the integration of 3D grade interpolation. Consequently, there is a significant opportunity to investigate the applicability of smartphone technology for subsurface geology applications including, but not limited to, comprehensive lithological mapping and enhanced geological modeling visualization.

2. Literature Review

2.1 Three-Dimensional Remote Sensing Reconstruction

The ability of traditional 3D reconstruction methods like TLS, MLS, and Structure-from-Motion Multi-View Stereo (SfM-MVS) to capture high-resolution data to create 3D digital

models is crucial to perform detailed analysis, visualization, and reality modeling (Di Stefano et al., 2021; Janiszewski et al., 2022; Singh et al., 2023). Different applications in urban environments, cultural heritage, environmental monitoring, agriculture, and underground environments, are among some of the most common contexts where the efficiency and accuracy of these techniques have been used to establish limits and challenges linked to environmental interferences, data density issues, and the need of human post-processing. It is common among studies to highlight the challenge posed by underground environments to facilitate the continuity and density of the data obtained through remote sensing techniques, referring to specific harsh conditions related to presence of moisture, dust, uniform colors, and inadequate illumination (Singh et al., 2023; Świerczyńska et al., 2024). Experimental studies and reviews of topographic, geological, and geotechnical underground mapping have found that while the use of TLS/MLS and SfM is effective for site assessments, such as change detection, clearance measurements, structural mapping, and tunnel digitization, these techniques also face specific technical constraints such as data transfer and georeferencing issues intervention (Huber and Vandapel, 2006; Di Stefano et al., 2021; Janiszewski et al., 2022; Singh et al., 2023).

Smartphone LiDAR and SfM technologies have gained significant interest and application, particularly in subterranean environments where the accuracy of smartphone-based LiDAR technology has been a focal point that has uncovered both potential and limitations. Studies often benchmark smartphone LiDAR against traditional techniques like TLS and SfM, noting that while smartphone LiDAR is less accurate (Rutkowski and Lipecki 2023; Świerczyńska et al., 2024), it is more user-friendly and cost effective (Torkan et al., 2023).

The effectiveness of smartphone LiDAR as a practical technology to create accurate 3D models is frequently evaluated in diverse underground mine-related applications. Mineshaft

sinking and tunnel measurements with rock engineering emphasis are examples of this tool´s versatility, proving its adaptability to be used in these type of challenging underground environments (Rutkowski and Lipecki 2023; Torkan et al., 2023), nevertheless occasionally deeming its results when performing certain measures, such as the estimation of convergence in mine chambers (Świerczyńska et al., 2024). Abbas and Abed (2024) established that for another non-mine related underground application, this technology proved to be very beneficial and flexible for recording small subsurface archaeological features, even outperforming terrestrial sensors. A frequent discussion about the trade-offs between accuracy and usability when using smartphone LiDAR can be found across studies, underscoring the importance of balancing precision with practicality in data acquisition (Rutkowski and Lipecki 2023; Torkan et al., 2023).

Smartphone based remote sensing techniques have also been explored in studies focused on surface applications such as geoscience (Luetzenburg et al., 2021; Tavani et al., 2022), urban planning/construction (Hou et al., 2024), and cultural heritage preservation (Teppati Losè et al., 2022; Błaszczak-Bąk et al., 2023), among others. The studies emphasized the existence of the same or additional potential/limitations associated with the creation of 3D models under distinct conditions such as lighting or material types, which might differ from those found in underground applications. While the convenience and ease of use of smartphone devices for rapid data acquisition make them particularly useful for preliminary data collection and educational purposes, this technology has often been found inadequate for detailed analytical tasks due to issues like drifting errors and lower precision (Tamimi 2022; Tavani et al., 2022). Despite the LiDAR sensor integrated into iPhones and iPads offering significant advantage in terms of accessibility; they are not sufficient for professional applications due to their lower accuracy and precision compared with those obtained with traditional surveying equipment like

total stations (Teppati Losè et al., 2022; Askar and Sternberg 2023), SfM (Luetzenburg et al., 2021) or when compared to advanced AR headsets (Hou et al., 2024). The Apple LiDAR is mainly valuable for quick assessments, especially in scenarios where traditional equipment may be impractical (Tavani et al., 2022; Błaszczak-Bąk et al., 2023). However, its limitations, under conditions such as poor lighting or reflective surfaces, necessitate further enhancements in the sensor´s technology, integration of additional stabilization along with the development of advanced data processing algorithms in software to reduce the variability identified in the performance of different apps (Tamimi 2022; Teppati Losè et al., 2022).

2.2 LiDAR Intensity

Lithological differentiation can be effectively achieved using LiDAR intensity data as demonstrated in several studies focused on obtaining such values using TLS over different materials and settings. This technique has been included across studies as the main component in different methods to either correct the intensity values to perform lithological mapping (Penasa et al., 2014; Carrea et al., 2016; Nováková et al., 2022), or to characterize rock properties and geological layers, especially in areas with restricted or no accessibility due to remote or hazardous terrain conditions (Burton et al., 2011; Humair et al., 2015). SfM, spectral analysis and computer vision are techniques that have been used to support intensity lithological differentiation demonstrating the effectiveness of integrating geometrical modeling, reflectance response, and machine learning derived information for lithological mapping and characterization (Penasa et al., 2014; Humair et al., 2015).

Studies have reported high success rates when applying lithological differentiation based in intensity response, indicating LiDAR´s potential for remotely mapping lithologies (Penasa et al., 2014; Humair et al., 2015; Carrea et al., 2016; Nováková et al., 2022). However, achieving

such precision may require specific weathering conditions and/or correcting LiDAR intensity data. Burton et al. (2011) experimented on unweathered core samples and lightly weathered outcrops focusing on clastic rocks. The authors noted the need for calibration to quantitative data and distance normalization. Penasa et al. (2014) developed a method for mapping chert in natural outcrops using intensity textures and local geometry descriptors. They corrected the data by adjusting it from distance effects. Humair et al. (2015) worked on differentiating between limestones layers. Their methodology focused on semi-automatically segmenting such lithologies based on intensity signatures and field observations to define thresholds. The authors were able to model the outcrop geometry accurately and quantify layer thickness variations. Carrea et al. (2016) used a reflectance correction model considering the influence of range, incidence angle, and surface properties on the recorded intensities. They used 10 blocks of different rock types such as marble, granite, sandstone, and chalk and found the correction to significantly reduced variability in intensities. Nováková et al. (2022) developed a workflow to correct LiDAR intensity considering the influence that moisture, acquisition geometry and surface properties had over intensity data obtained from cave rocks (marble and lherzolite).

2.3 Spatial Representation: Point Cloud Density Estimation and Interpolation

Point cloud density estimation is a technique used to measure the spatial resolution and quality of 3D point clouds, and it assesses the accuracy and reliability of 3D models. Torkan et al. (2023) used point cloud densities to evaluate the accuracy of 3D tunnel models reconstructed using SfM and smartphone-based LiDAR. They calculated the cloud-to-cloud absolute distance between the reference point cloud obtained through SfM and the LiDAR models, finding SfM more accurate and concluding that LiDAR remained a viable method when high precision is not required. Rutkowski and Lipecki (2023) used point cloud density to validate the accuracy of the

iPhone 13 Pro LiDAR scanner against professional LiDAR equipment. They computed cloud-to-cloud distances finding that the iPhone 13 Pro's point cloud density, though lower, was sufficiently accurate for practical applications, with a manageable difference in accuracy.

Spatial interpolation is another key technique used to incorporate geological information into the content and visualization of underground mine 3D models (Peters, 1993; Nwaila et al., 2024). Methods like IDW, kriging, and machine learning approaches can significantly enhance the accuracy of geological models by filling in gaps where sample data may be sparse. Nwaila et al. (2024) highlighted the advantages of using machine learning techniques for spatial interpolation, noting that these methods can capture patterns and regularities that traditional techniques might lose. Peters (1993) discussed the application of spatial interpolation methods, specifically IDW, for understanding the spatial variability and continuity of gold grades in gold-quartz vein deposits. In his study, the deposit was divided into blocks, and values were assigned based on the surrounding sample data, allowing for the characterization of the erratic variations in vein width and continuity of mineralization. Nwaila et al. (2024) underscored that while advanced methods like machine learning can provide more nuanced models, simpler methods like IDW still hold value for their ease of use and interpretability in complex geological settings. The selection of an interpolation method should be guided by the specific geological context and the nature of the available data (Peters, 1993; Nwaila et al., 2024).

3. Methodology

3.1 Study Area Description

La Independencia underground mine, a gold and silver deposit owned by Denarius Metals, a Canadian mining and exploration company, is situated on the western side of the Central Cordillera (Andes). Figure 1 locates the mine at multiple scales: within Colombia, the

Department of Antioquia, and specifically in the Municipality of Titiribí, approximately 56.8 km southwest of Medellín, Colombia's second-largest city.

Figure 1. Map of the study area: La Independencia Mine.

3.2 Data Source

The data used in this research is categorized into primary and secondary sources (Table 1). The raw data was self-surveyed and collected in the field, while the processed primary data resulted from analyzing the raw data using the tools indicated in Table 1. Secondary data, provided directly by the chief geologist at Denarius Metals, was further processed to create additional outputs. This secondary data is proprietary to Denarius Metals and was made accessible exclusively for this project under a collaborative agreement (not publicly accessible).

Table 1. Data source summary. *ply - Polygon File Format, png - Portable Network Graphics, pts - Point Cloud Format, dwg - Drawing, las - LASer File Format, slpk - Scene Layer Package, obj - Object File Format, shp - Shapefile, xlsx - Excel Spreadsheet Format, vtk - Visualization Toolkit, mp4 - Moving Picture Experts Group-4 Part 14, jpg - Joint Photographic Experts Group. *Not open-source tools.*

Category	Type of Data	Source/Tool	Quantity: Format
Primary Data (Raw)	**LiDAR RGB Point Cloud**	*Polycam	3: ply – pts – las
	Textured Mesh	*Polycam	2: obj – ply
	RGB Photos	RTAB-Map	1,342: jpg
	Depth Photos	Polycam	753: png
		RTAB-Map	1,342: png
	RGB Video	Stray Scanner	1: mp4
Primary Data (Processed)	**RGB Point Clouds**	RTAB-Map Desktop	3: ply – pts – las
		StrayVisualizer	3: ply – pts – las
		*ArcGIS Pro	1: slpk
	Extracted RGB Photos	StrayVisualizer (Python)	1932: jpg
	RGB Point Cloud	Meshroom	1: ply
	Textured Meshes	RTAB-Map Desktop/ MeshLab	1: ply
		Meshroom	1: obj
	RGB - Mesh	StrayVisualizer	1: ply
	Interpolated Meshes	PyVista	3: vtk
		Paraview	3: ply
Secondary Data	**Topography Layers**	Denarius Metals	1: dgw
	Topography Stations		1: xlsx
	Sampling Database		1: xlsx
Secondary Data (Processed)	**Mine Topography**	*ArcGIS Pro	1: shp
	Mine Adit		1: shp
	Rock Samples		1: shp

3.3 Methodology Overview

The methodology for creating and analyzing a geologic 3D model of the La Independencia underground mine comprises three main stages: data acquisition, data processing, and data visualization. Figure 2 presents the workflow between stages.

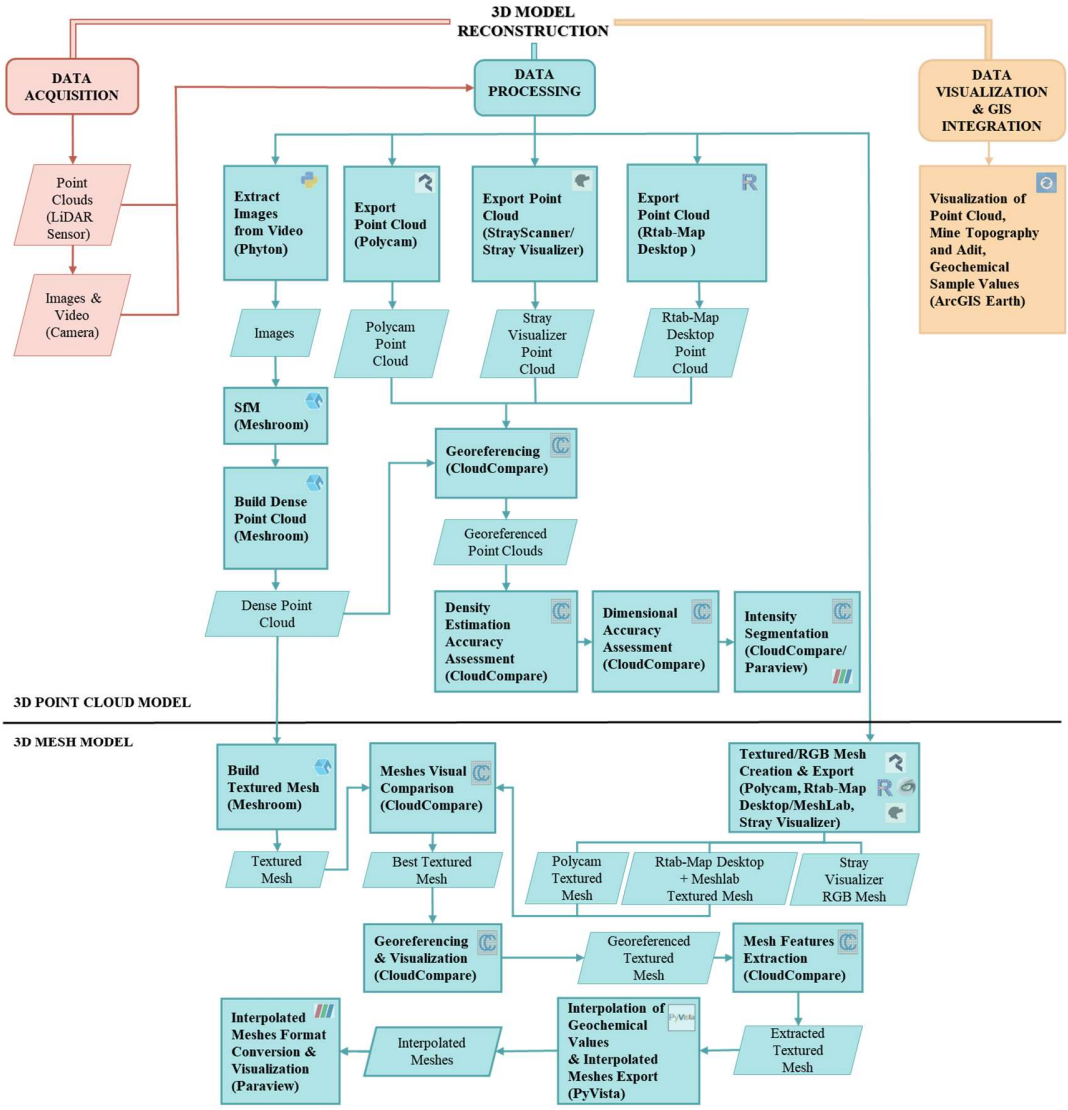

Figure 2. Methodology flow chart.

3.4 Data Acquisition and Equipment

As indicated in Figure 3a, La Independencia mine includes a crosscut extending 729 m in the direction of 254°, with other sections present above the Independencia level (Level 0). The data acquisition phase was carried out in a 24-meter section surveyed at Level 0 (975 masl) of a horizontal drift (Colmena West) within the mine. This specific location corresponds to where all the fieldwork and analysis for this research project took place.

The primary device for data collection was an iPhone 13 Pro equipped with a LiDAR sensor and attached to a gimbal rig for stabilization and an integrated lighting setup consisting of two cordless 10,000-lumen LED lights (Figure 3b). This setup ensured proper illumination and prevented gradual misalignments that can distort 3D data (drift errors) during scanning.

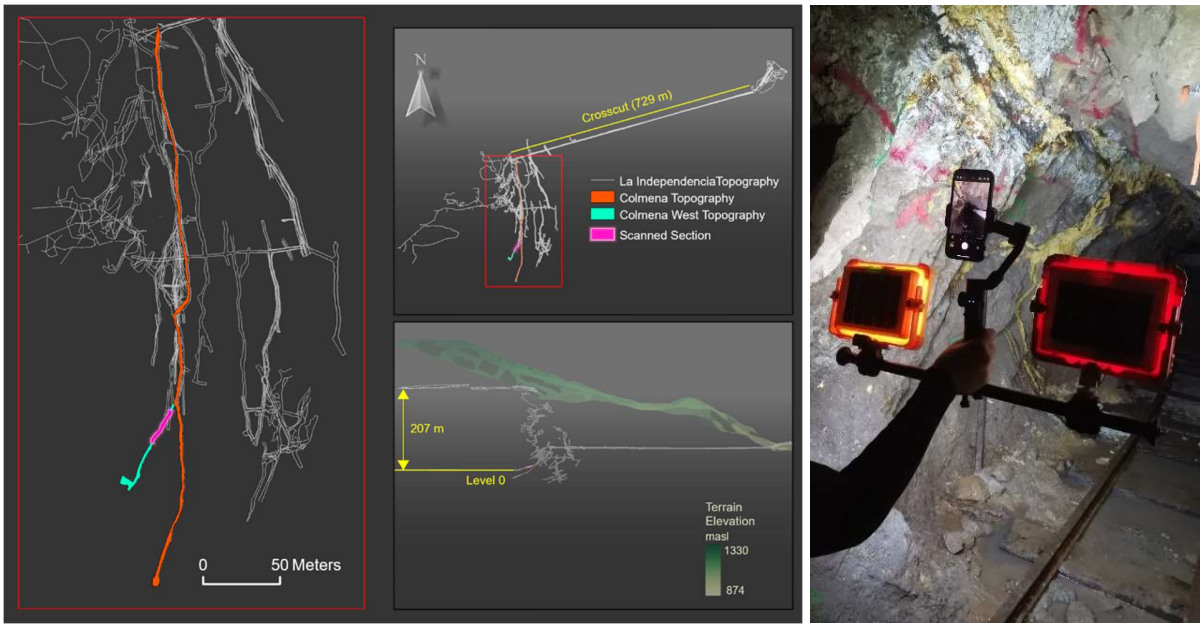

(a) (b)

Figure 3. Data acquisition location and equipment: (a) Surveyed section map – Colmena West, (b) iPhone gimbal rig with lighting setup.

3.5 Scanning Procedure

In June 2024, the selected mine section was scanned using the commercial app Polycam (selected for its reliable reality capture) and two free apps: RTAB-Map (with advanced settings for capture and processing control) and Stray Scanner (alongside with depth capture, supports video recording for SfM post-processing). Each app was used to capture LiDAR and RGB data for generating 3D point clouds and visual media. The aim was to explore and compare these apps based on their usability and source type (commercial vs. non-commercial).

The scanning process was performed with the iPhone held upward to maximize height coverage. A single pass through the section using each app was conducted without a specific

path or mapping strategy, relying on pre-inspection to identify any obstructions and ensure ease of mobility. Each of the three scans started from the first Ground Control Point (GCP) and covered as many angles as possible of the walls, roof, and floor to capture the quartz vein details accurately and other elements inside the section. Slow and steady movements were maintained to minimize drift errors, and care was taken to avoid re-scanning the same areas multiple times. Each scan continued until the third control point was reached. In the scanning procedure for the Polycam app, the "LiDAR mode" was selected as the scanning method, generating a pre-mesh based on the iPhone's LiDAR sensor with a range of up to 5 meters from each scanning position. This mode allows for capturing photographs while scanning. The RTAB-Map app included a real-time preview displaying the point cloud generation on the iPhone screen and provided the option to either proceed with graph optimization and mesh assembly or simply save the session. The latter option was chosen, allowing for mesh generation at a later time using RTAB-Map Desktop and MeshLab. Finally, the Stray Scanner app offered minimal user configuration, operating with default high-definition camera settings. The interface displayed a video on the screen as the scan progressed capturing RGB video and depth data simultaneously.

3.6 Data Processing

3.6.1 Image Extraction, Export and Georeferencing

After rotating the RGB video obtained with the Stray Scanner app by 90°, a total of 1,932 high-definition (1440x1920) images were extracted using a custom Python script that utilized standard and not specialized libraries.

For the export, las, ply, and pts formats were used across applications for compatibility with ArcGIS Pro (las), versatility in 3D modeling (ply), and to retain intensity values (pts). Polycam exported the point cloud directly via the app's built-in export options, selecting three

different formats: las, ply, and pts. RTAB-Map generated a database file (db) for the scanning session containing all recorded data. This file was imported into RTAB-Map Desktop to save the point cloud in ply and pts formats. The StrayVisualizer tool was used to process the Stray Scanner data saving the point cloud in ply and pts formats. A fourth point cloud was created using the Meshroom´s SfM pipeline using the 1,932 images extracted from the Stray Scanner RGB video to reconstruct a dense 3D point cloud which was saved in ply and pts formats.

All point clouds were georeferenced using CloudCompare. The georeferencing process utilized three GCPs well-distributed across the scanned area and located on the roof of the mine section, each with known UTM 18 N coordinates.

3.6.2 Accuracy Assessment

CloudCompare was used to evaluate the four point clouds' completeness (via surface density estimation) and dimensional precision (through dimensional accuracy methods). Before performing surface density estimation, the point cloud generated using Meshroom was cleaned to remove dispersed points, as the raw point cloud contained considerable noise. The density estimation technique highlighted variations in point sampling across the four-point clouds. This comparison was essential for evaluating the completeness and resolution of the point clouds. To estimate the surface point density of each point cloud the same local neighborhood radius (r = 0.01 meters) was selected to ensure that the results were comparable. During the data collection stage, three specific locations within the mine were randomly selected to manually measure the thickness of the quartz vein leaving spray painted marks on the mine´s walls serving as visual records for such values. These real-world measurements were later compared to the thickness values extracted from the point clouds to assess the dimensional accuracy of each model.

3.6.3 Intensity Segmentation

The intensity values recorded by the LiDAR sensor during the scanning process were visualized using CloudCompare and ParaView. The point clouds exported in pts format were loaded into CloudCompare, which recognized the intensity values as a scalar field. The intensity values were adjusted to create a color gradient that visually emphasized the variations in intensity across the point cloud. By modifying the color scale, high- and low-intensity regions became more distinguishable, allowing for clearer visualization of different geological features.

3.6.4 Mesh Export

With Polycam, a textured mesh was exported directly via the app's built-in export options once the processing step was completed. The custom settings chosen for processing were “Depth range” 5 meters, “Voxel size” 21 mm, and “Simplification” 0%. The “Automatic crop” and “Loop closure” options were disabled. Another mesh was created using RTAB-Map Desktop and textured using MeshLab which was also used to export it in ply and obj formats. For Stray Scanner**,** the mesh was processed using the StrayVisualizer tool. An RGB-colored mesh was created and exported as a ply format for further analysis. Meshroom was used for the creation of the fourth textured mesh via the SfM pipeline. The “Texturing” node was applied to take the dense 3D point cloud, camera images, and depth maps to generate a textured mesh. The resulting mesh was stored in obj format with its associated textures (jpg).

3.6.5 Visual Comparison and Georeferencing

A visual comparison of the textured meshes was performed to evaluate the quality, completeness, and smoothness of the reconstructed models. Since StrayVisualizer did not generate a textured mesh (only an RGB-colored mesh), the comparison was limited to meshes generated using Polycam, RTAB-Map Desktop, and Meshroom. The meshes were inspected for

their visual quality focusing on how well the images were projected onto the 3D geometry, with particular attention to the quartz vein due to its geological relevance. The comparison also used the meshes completeness remarking the amount of coverage and consistency in texture across the entire mesh, noting any gaps, missing areas, or distorted regions in the textures. One textured mesh was selected for further analysis and integrated into the next steps of the study. This selection was based on the chosen's mesh high visual quality and geometric accuracy.

Once the best-quality textured mesh was selected based on the visual comparison and accuracy assessment, the next step involved georeferencing the mesh using CloudCompare, following the same approach as used for the point clouds.

3.6.6 Mesh Extraction and Interpolation

The georeferenced mesh was used to extract the quartz vein as an independent mesh for further analysis. CloudCompare was employed to isolate the quartz vein from the rest of the mesh and export it as a ply file for further analysis and integration with other datasets.

To integrate sparse observational geochemical data (gold, silver, copper values) onto the extracted quartz vein mesh, the PyVista library was used to perform IDW interpolations. Using PyVista's "interpolate" filter, the geochemical point data was resampled across the surface of the mesh. A radius of 4.0 (the approximate distance between samples) was used to control the interpolation's spatial influence. After completing the interpolation, the mesh, along with the interpolated scalar values, was saved in vtk format. To ensure compatibility with CloudCompare, which does not support vtk files, the vtk mesh was then exported as ply using Paraview. The three interpolated meshes (Au, Ag, Cu) were imported into CloudCompare and integrated with the quartz vein extracted from the main model to create a final 3D Mesh Model.

3.7 Data Visualization and GIS Integration

The final step of the workflow involved visualizing the most complete and accurate 3D point cloud alongside other GIS data in shp format (mine topography, adit, geochemical sample values), using ArcGIS Earth (open source). To integrate the point cloud into ArcGIS Earth, it was necessary to assign spatial reference information (Projected Coordinate System and DATUM) to the point cloud file (las), previously aligned using CloudCompare. This was done using ArcGIS Pro, where the geoprocessing tools "Define Projection" and "Create Point Cloud Scene Content" were used. The point cloud was then converted into slpk format and loaded into ArcGIS Earth for interactive exploration including additional shapefiles overlayed on it.

4. Results and Discussion

4.1 Data Acquisition

Table 2 shows the total scanning time for each of the three apps used during fieldwork. Stray Scanner invested the least amount of time, followed by Polycam, and RTAB-Map taking the longest. This variation in duration reflects differences in each app's capture approach, which might have influenced the quality of the final point clouds produced by each application.

Table 2. Scanning time during data acquisition.

Mobile Application	Scanning Time (minutes)	Scanning Time (seconds)
Polycam	14	56
RTAB-Map	23	43
Stray Scanner	6	55

4.2 Export and Georeferencing

Figure 4 presents all four point clouds after export and georeferencing using the GCPs (ZM: 267-268-269), allowing for a visual comparison of their spatial alignment, coverage, and completeness. Figure 5 details the interior for each of the exported scanned point clouds.

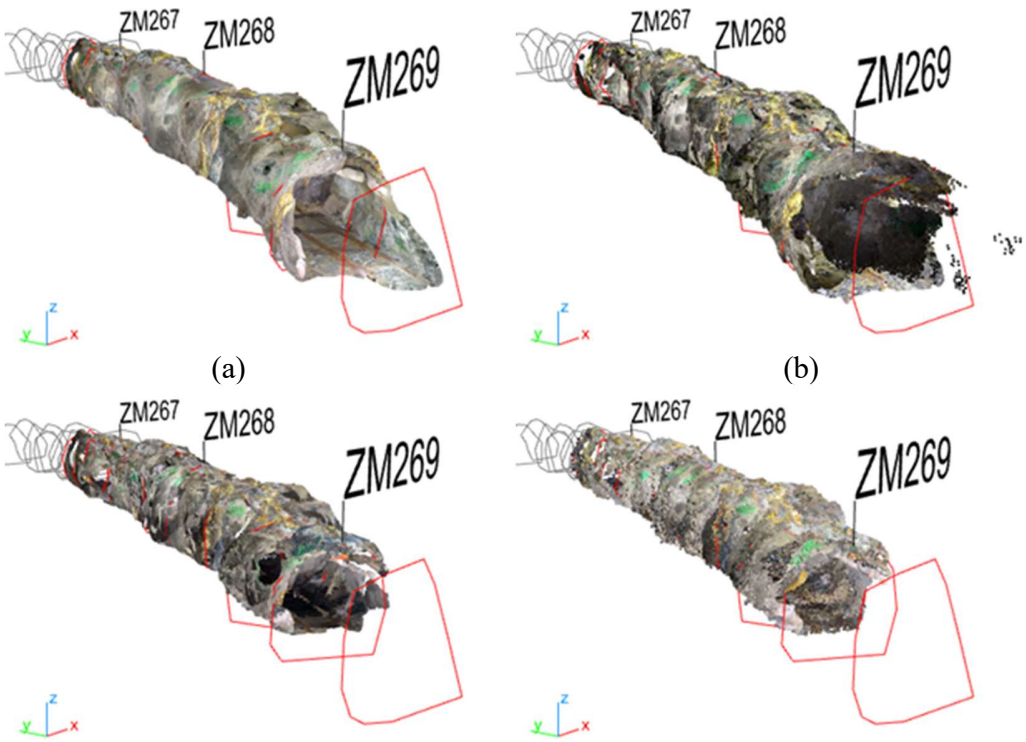

Figure 4. Aligned point clouds: (a) Polycam, (b) RTAB-Map, (c) Stray Scanner, (d) Meshroom.

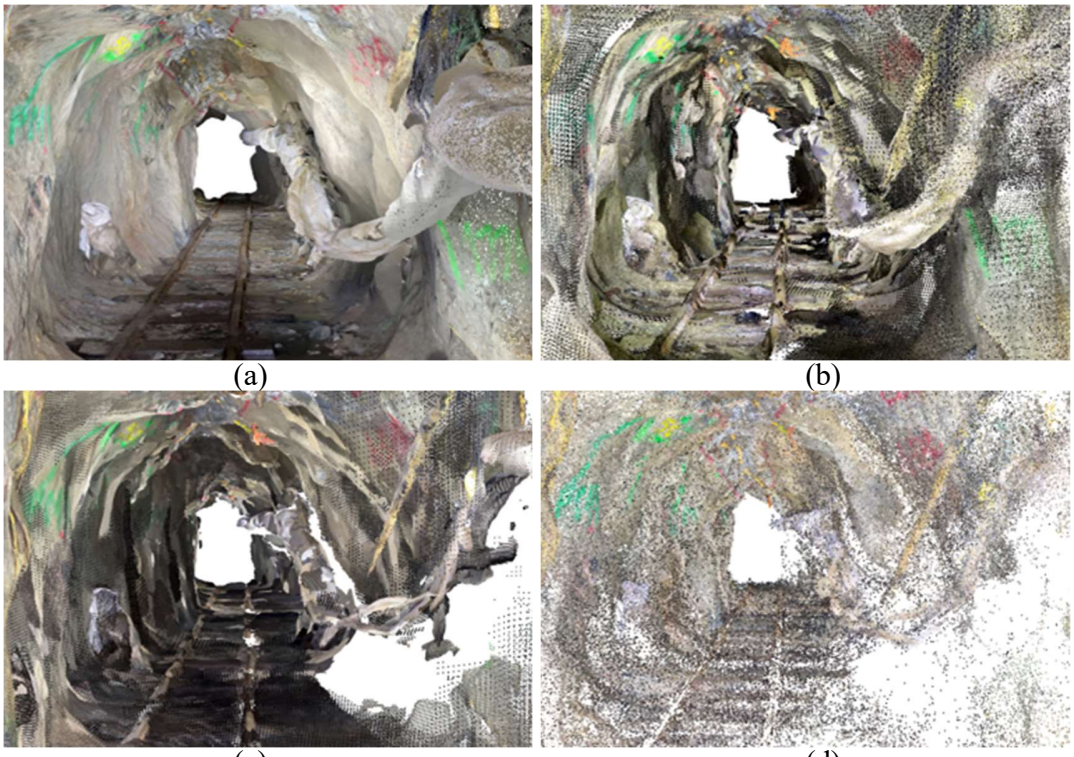

Figure 5. Point cloud detail: (a) Polycam, (b) RTAB-Map, (c) Stray Scanner, (d) Meshroom.

4.3 Accuracy Assessment

Table 3 presents the georeferencing RMS error and mean surface point density. All point clouds exhibited low RMS error values, indicating accurate georeferencing to the real-world mine section. Figure 6 illustrates the surface density of each 3D point cloud and the distribution of points across the surface. Polycam showed the highest point density, capturing a very detailed point cloud. In comparison, RTAB-Map displayed lower overall density. Stray Scanner had varied density and a relatively high standard deviation (Table 3), indicating uneven point distribution. In contrast, Meshroom produced the lowest density (sparsest point cloud).

Table 3. 3D point clouds georeferencing RMS error and mean surface point density.

Application (Method)	Point Count	RMS error (m)	Mean Point Density (point/m^2)	Standard Deviation
Polycam (LiDAR)	16,531,150	0.04	80,219	12,748
RTAB-Map (LiDAR)	4,348,258	0.08	9,808	4,797
Stray Scanner (LiDAR)	8,347,579	0.008	121,070	175,477
Meshroom (SfM)	1,903,480	0.01	50,669	69,382

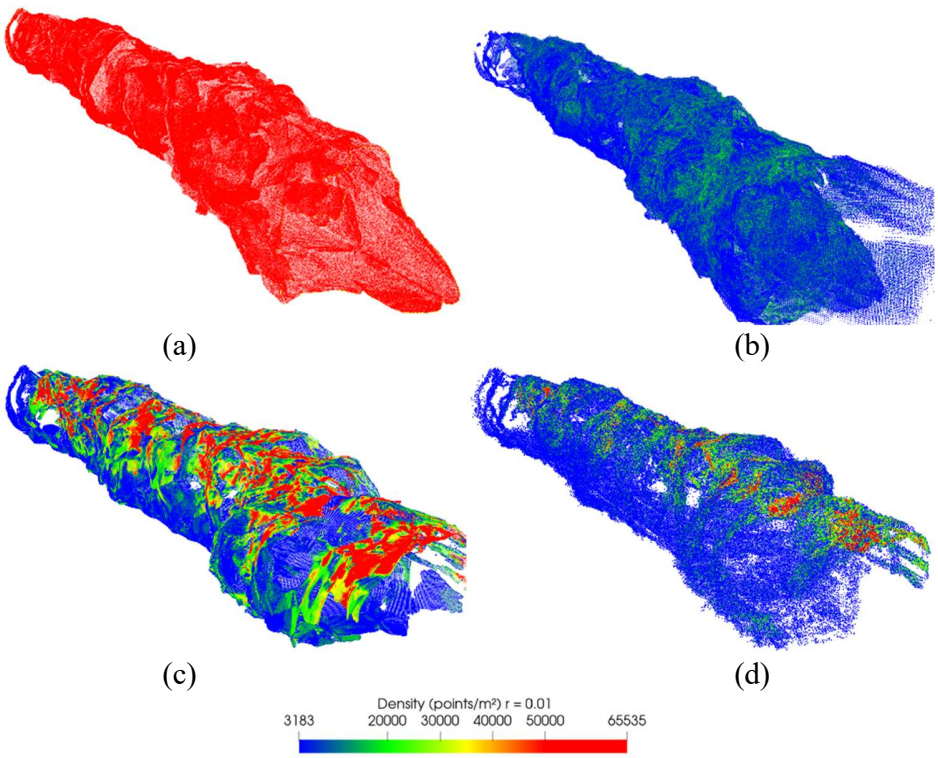

Figure 6**.** Point cloud density. (a) Polycam, (b) RTAB-Map, (c) Stray Scanner, (d) Meshroom.

Table 4 compares quartz vein thicknesses between field measurements and the Polycam 3D Point Cloud model showing a perfect match across all points. These results indicate that the Polycam 3D model accurately represents the quartz vein thickness.

Table 4. Quartz vein thickness: In-field and 3D model measurements comparison.

Point	In Field Measure (m)	3D Point Cloud Model Measure (m)	Difference (m)
1	0.56	0.56	0
2	0.50	0.50	0
3	0.55	0.55	0

Figure 7 provides a visual comparison of quartz vein thickness between the field and the 3D model generated using Polycam. The top images display the thickness measurements taken from the 3D model, while the bottom images correspond to field photos. The yellow numbers spray painted on the mine walls were the measurements taken during field work.

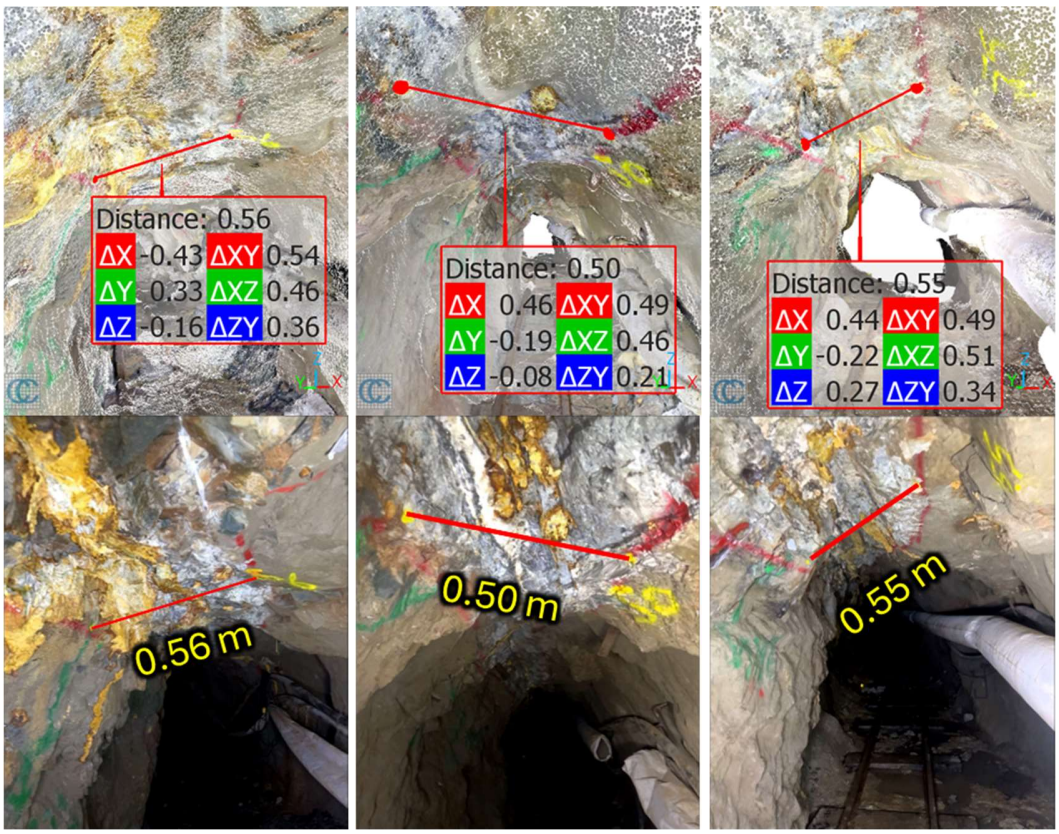

(a) (b) (c)

Figure 7. Quartz vein thickness measurements: (a) Point 1, (b) Point 2, (c) Point 3.

4.4 Intensity Segmentation

The segmentation of the 3D point cloud using LiDAR intensity values successfully identified zones where higher intensity responses correlate with key geological features. As established in Figure 8, the primary quartz vein exhibited a strong intensity response, enabling its clear delineation from the surrounding host rock. In addition, areas with elevated intensity beyond the main vein were observed, likely corresponding to fault zones, secondary veins or alteration halos where the host rock has been affected by fluid interactions.

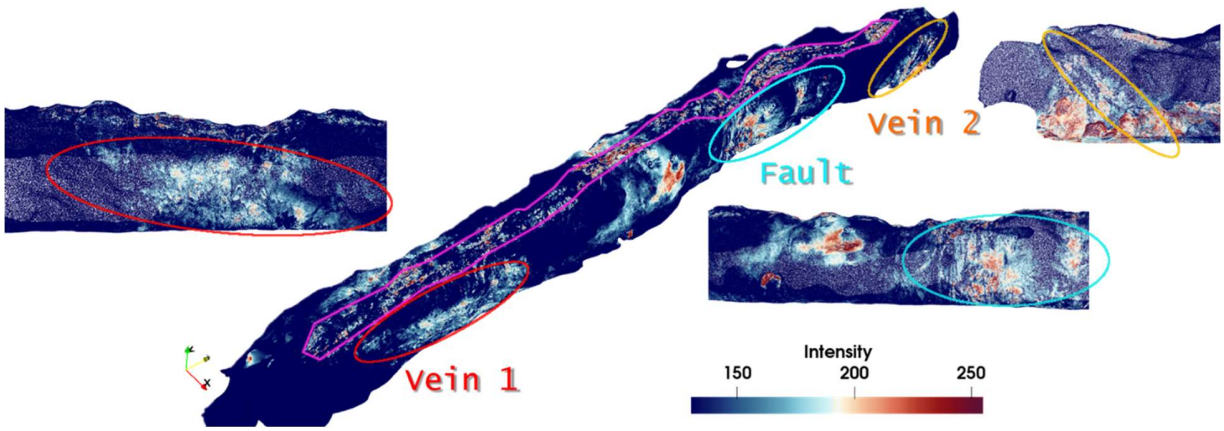

(a)

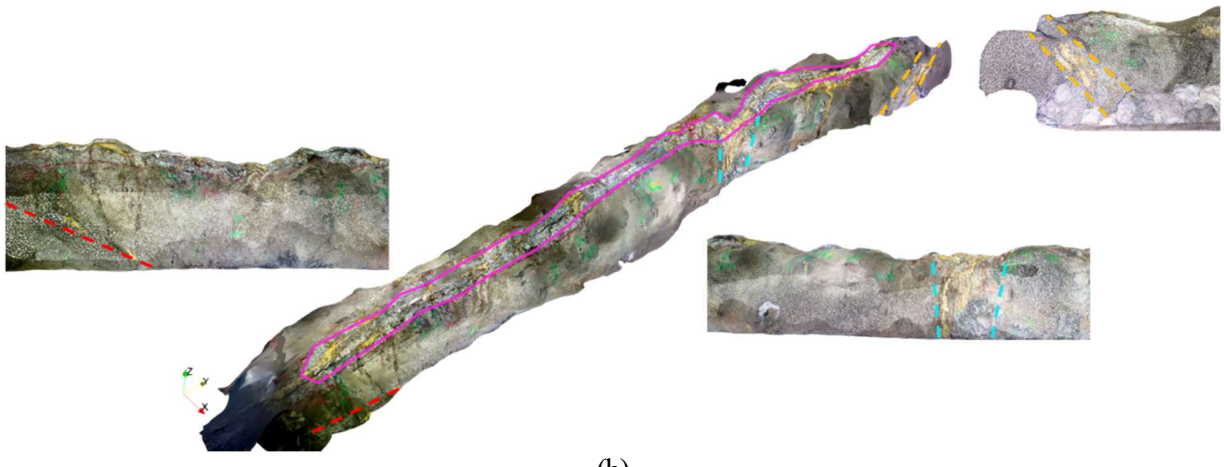

(b)

Figure 8. Polycam 3D point cloud: (a) colored by intensity, (b) colored by RGB.

However, as noted in Figure 9, it is important to annotate those other non-geological elements such as sandbags and ventilation ducts, that also display high-intensity values.

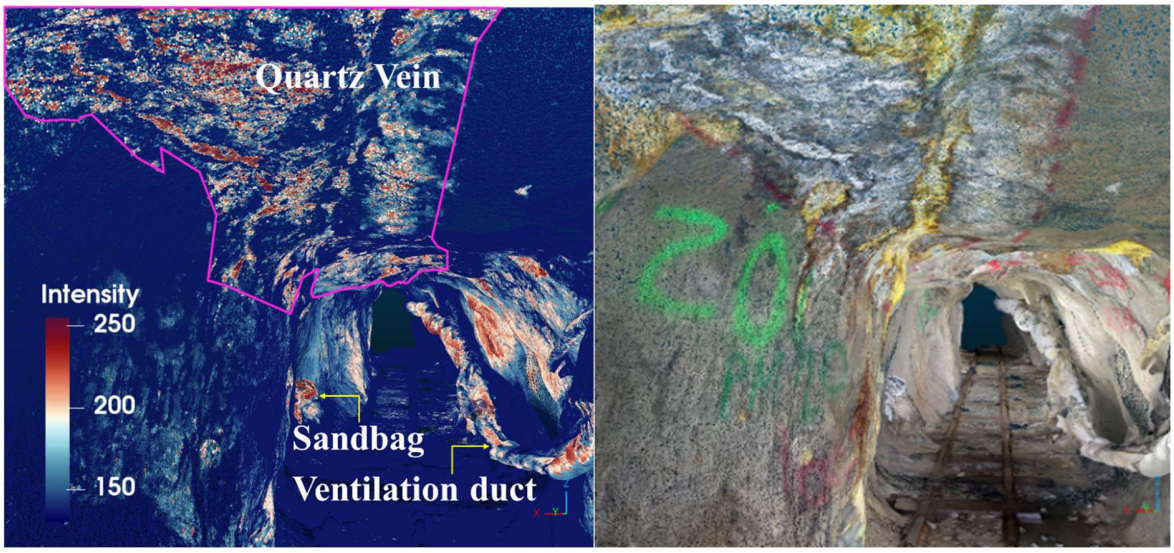

(a) (b)

Figure 9. Intensity response: a) Polycam´s point cloud intensity, b) Polycam´s RGB point cloud.

4.5 Mesh Export

Four 3D mesh models were created. Stray Visualizer produced the only RGB-colored mesh without textures. The variations in processing and acquisition approaches contributed to differences in detail across the models (Figure 10).

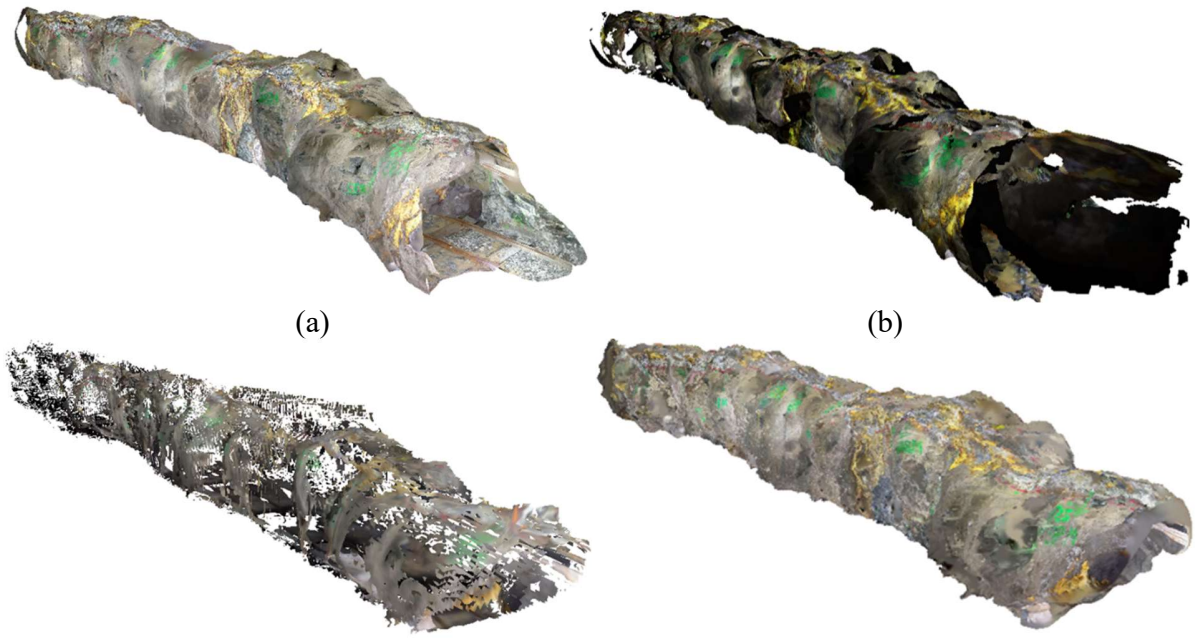

(a) (b)

(c) (d)

Figure 10. 3D Mesh Models: (a) Polycam, (b) RTAB-Map, (c) Stray Scanner, (d) Meshroom.

4.6 Visual comparison and Mesh Extraction

Figure 11 presents a closer view of the resultant meshes. The Polycam app (Figure 11a) generated the most complete, visually appealing, and sharp 3D textured mesh, reason why it was used for segmenting out the Colmena West quartz vein (Figure 11d).

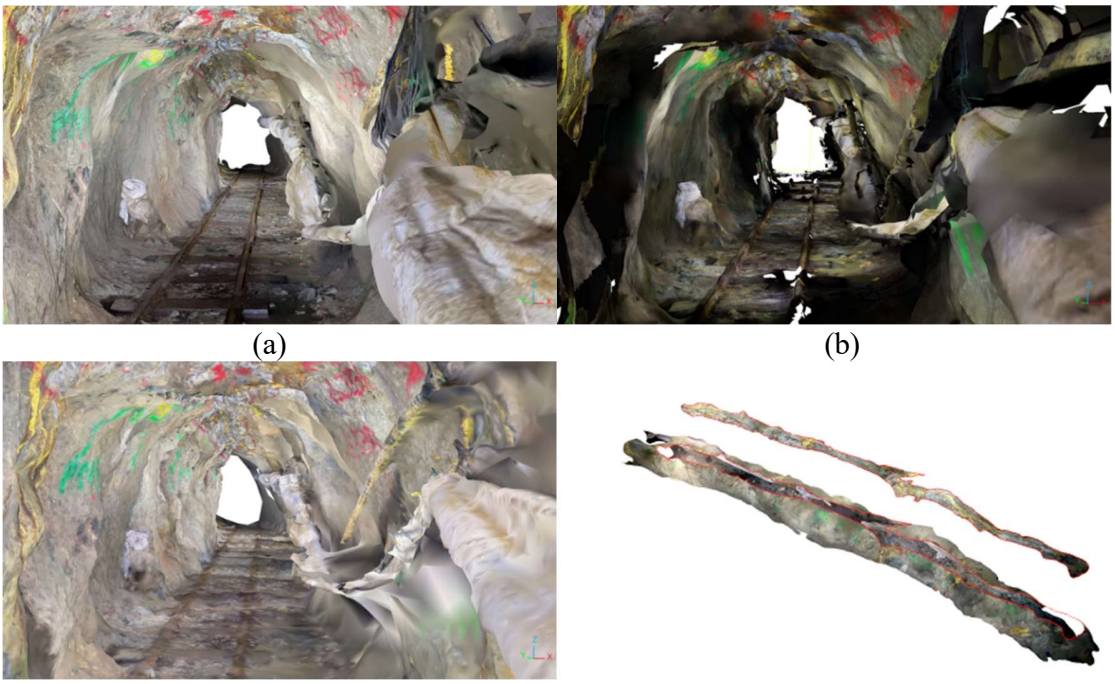

(a) (b)

(c) (d)

Figure 11. Mesh comparison: (a) Polycam, (b) RTAB-Map, (c) Meshroom. (d) Polycam 3D mesh model / extracted Colmena West quartz vein.

4.7 Interpolation

PyVista combined the Polycam´s extracted mesh with interpolated geochemical data offering a comprehensive and detailed representation of the spatial variation of Au, Ag, and Cu across the quartz vein. Figure 12 presents the integration of the interpolated geochemical data (Au-Ag-Cu meshes) with Polycam's 3D textured mesh. This detailed visualization facilitates a deeper understanding of how the distribution of Au, Ag, and Cu values correlates with the geological features within the scanned section. The integration also allowed for a better understanding of how geological relationships influence metal distribution.

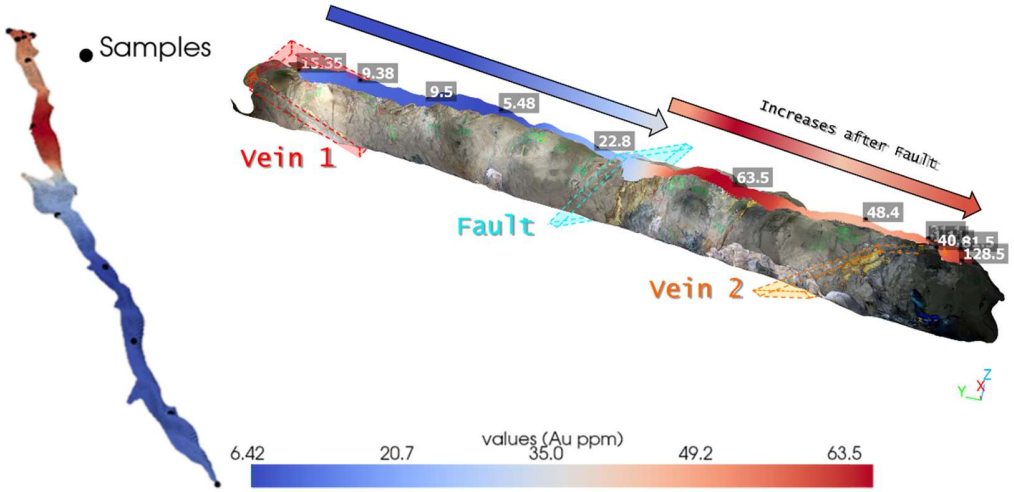

(a)

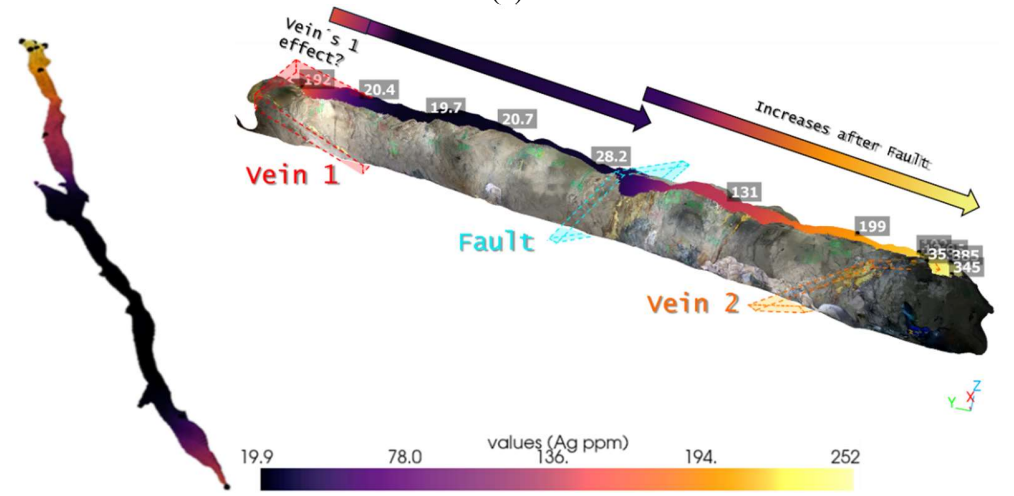

(b)

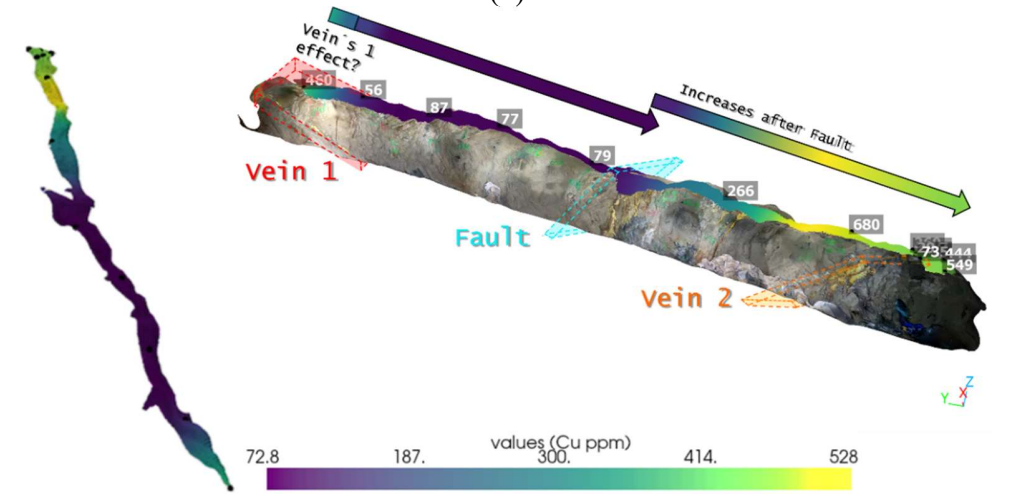

(c)

Figure 12. PyVista interpolated meshes integrated with Polycam's 3D mesh model: (a) Gold - Au, (b) Silver - Ag, (c) Cupper - Cu.

The proximity of Vein 1 (Figure 13a) appears to correlate with elevated Ag and Cu concentrations near its intersection with the primary Colmena West quartz vein, indicating structural control on mineralization. Additionally, a fault (Figure 13b) in the scanned section shows a notable increase in Au, Ag, and Cu values, particularly where Vein 2 (Figure 13c) intersects the Colmena W (West) quartz vein. These patterns underscore the role of faulting and intersecting veins in enhancing geochemical values, providing insights into mineralization processes in the deposit.

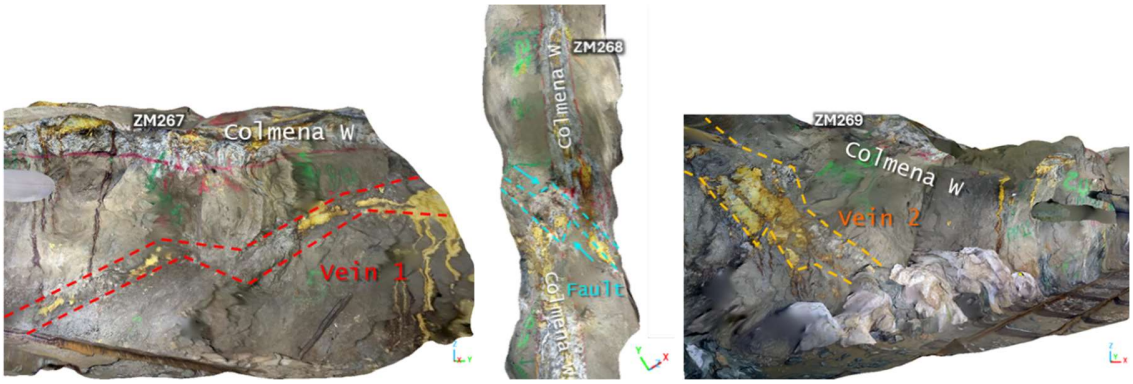

(a) (b) (c)

Figure 13. Structural controls on mineralization: (a) Vein 1, (b) Fault, (c) Vein 2.

4.8 Data Visualization and GIS Integration

Figure 14 presents a detailed cartographic view of the La Independencia mine surveyed section, created using ArcGIS Earth and integrating other GIS data to achieve a comprehensive 3D representation. The visualization includes elements such as the quartz vein in relation to geochemical data and non-geological features, based on the 3D point cloud model generated in previous steps. This approach enabled a thorough assessment of the reconstructed 3D model, providing an interactive spatial context while leveraging the high-resolution rendering capabilities of the software.

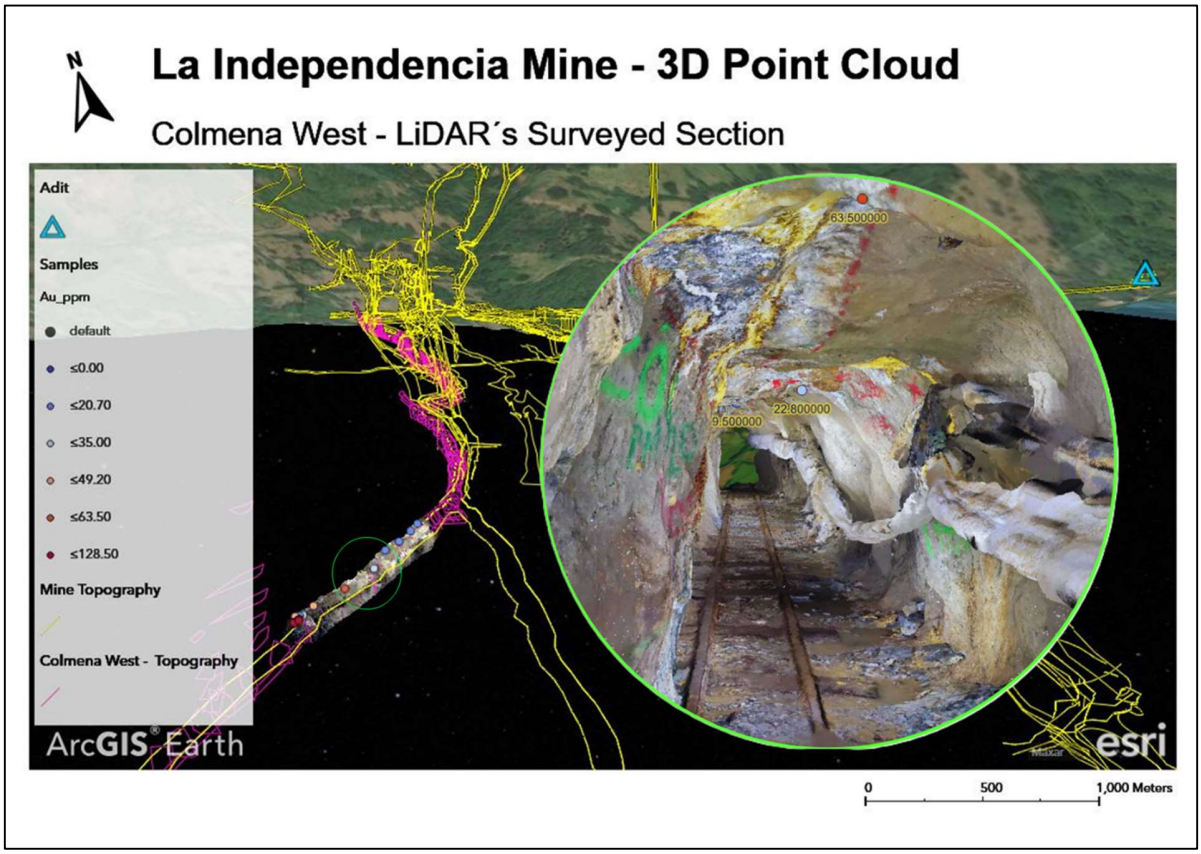

Figure 14. La Independencia scanned mine section as a 3D point cloud model in ArcGIS Earth.

4.9 Limitations

During the intensity segmentation of the quartz vein, elements such as sulfur and clay created low responses disrupting the continuity of the vein. This highlighted the difficulty in obtaining a continuous segmentation of the geological structure. Similarly, non-lithological features presented high-intensity responses comparable to the one obtained for the quartz vein. For the interpolation of geochemical data, sampling coordinates provided as secondary data had to be adjusted to match the quartz vein location. Another issue was that sparse sampling points posed a challenge in producing a continuous and reliable representation of mineral grades. To address this, the interpolation ratio (r) value had to be carefully selected, ensuring that the mineral grade representation remained as accurate as possible despite the limited data points.

5. Conclusion

This research successfully met its primary objective of utilizing affordable and open-source tools to create and visualize geological 3D models of an underground mine in Titiribí, Colombia. The study employed smartphone-based LiDAR and photogrammetry to generate 3D point clouds and meshes of a 24-meter section of the La Independencia Mine. Data was collected using Polycam, RTAB-Map, and Stray Scanner apps, while secondary data was externally provided. Processing involved image extraction to apply SfM, point cloud georeferencing, and assessments of density, accuracy, and intensity. Meshes were exported, visually compared, and georeferenced, with additional interpolation of geochemical values onto an extracted mesh, leading to a final 3D mesh model. Integration in ArcGIS Earth enabled comprehensive visualization and interactive exploration of the 3D point cloud model.

The data acquisition and density results demonstrated that accuracy differences were influenced not only by scanning time and capture approach but also by the internal processing capabilities of each application, with Polycam producing a denser point cloud despite investing less scanning time than RTAB-Map. Polycam's high density and accurate quartz vein thickness measurements confirmed its suitability for geological modeling. Geochemical data integration revealed faults and intersecting veins influencing metal distribution. However, intensity-based segmentation was hindered by clay and sulfur content and non-lithological high-intensity responses. These findings demonstrate that while smartphone-based tools are accessible and effective for rapid data acquisition and visualization, further advancements are needed to address segmentation challenges. Future research should prioritize improving intensity segmentation methods, integrating advanced machine learning techniques to effectively address automated segmentation and lithological mapping challenges within 3D virtual models.

References

Abbas, S.F. and Abed, F.M., 2024. Revolutionizing Depth Sensing: A Review study of Apple LiDAR sensor for as-built scanning Applications. *Journal of Engineering*, *30*(04), pp. 175–199.

Askar, C. and Sternberg, H., 2023. Use of Smartphone LiDAR Technology for Low-Cost 3D Building Documentation with iPhone 13 Pro: A Comparative Analysis of Mobile Scanning Applications. *Geomatics* (2673-7418), 3(4), pp. 563–579.

Błaszczak-Bąk, W., Janicka, J., Dumalski, A., and Masiero, A., 2023. Integration of terrestrial laser scanning and smartphone LiDAR: The case study of Lidzbark Castle. *International Archives of the Photogrammetry, Remote Sensing and Spatial Information Sciences,* XLVIII-1/W1-2023, pp. 51–56.

Burton, D., Dunlap, D.B., Wood, L.J. and Flaig, P.P., 2011. LiDAR intensity as a remote sensor of rock properties. *Journal of Sedimentary Research*, 81(5), pp.339–347.

Carrea, D., Abellan, A., Humair, F., Battista, M., Derron, M.H., and Jaboyedoff, M., 2016. Correction of terrestrial LiDAR intensity channel using Oren–Nayar reflectance model: An application to lithological differentiation. *ISPRS journal of photogrammetry and remote sensing*, 113, pp. 17–29.

Di Stefano, F., Chiappini, S., Gorreja, A., Balestra, M., and Pierdicca, R., 2021. Mobile 3D scan LiDAR: A literature review. *Geomatics, Natural Hazards and Risk*, 12(1), pp. 2387.

Hou, J., Hübner, P., Schmidt, J., and Iwaszczuk, D., 2024. Indoor Mapping with Entertainment Devices: Evaluating the Impact of Different Mapping Strategies for Microsoft HoloLens 2 and Apple iPhone 14 Pro. *Sensors* [online], 24(4), 1062. Available from: https://doi.org/10.3390/s24041062.

Huber, D.F. and Vandapel, N., 2006. Automatic 3D underground mine mapping. *The International Journal of Robotics Research*, 25(1), pp. 7–17.

Humair, F., Abellan, A., Carrea, D., Matasci, B., Epard, J. and Jaboyedoff, M., 2015. Geological layers detection and characterization using high resolution 3D point clouds: Example of a box-fold in the Swiss Jura Mountains. *European Journal of Remote Sensing*, 48(1), pp. 541–568.

Janiszewski, M., Torkan, M., Uotinen, L. and Rinne, M., 2022. Rapid photogrammetry with a 360-degree camera for tunnel mapping. *Remote Sensing* [online], 14(21), p.5494. Available from: https://doi.org/10.3390/rs14215494.

Luetzenburg, G., Kroon, A., and Bjørk, A.B., 2021. Evaluation of the Apple iPhone 12 Pro LiDAR for an Application in Geosciences. *Scientific Reports*, 11(1), pp. 1–9.

Nováková, M., Gallay, M., Šupinský, J., Ferré, E., Asti, R., de Saint Blanquat, M., Bajolet, F. and Sorriaux, P., 2022. Correcting laser scanning intensity recorded in a cave environment for

high-resolution lithological mapping: A case study of the Gouffre Georges, France. *Remote Sensing of Environment* [online], 280, p.113210. Available from: https://www.sciencedirect.com/science/article/abs/pii/S0034425722003182?via%3Dihub.

Nwaila, G.T., Zhang, S.E., Bourdeau, J.E., Frimmel, H.E. and Ghorbani, Y., 2024. Spatial Interpolation Using Machine Learning: From Patterns and Regularities to Block Models. *Natural resources research*, 33(1), pp. 129–161.

Penasa, L., Franceschi, M., Preto, N., Teza, G., and Polito, V., 2014. Integration of intensity textures and local geometry descriptors from terrestrial laser scanning to map chert in outcrops. *ISPRS Journal of Photogrammetry and Remote Sensing*, 93, pp. 88–97.

Peters, S., 1993. Formation of oreshoots in mesothermal gold-quartz vein deposits: examples from Queensland, Australia. *Ore Geology Reviews*, 8(3–4), pp. 277–301.

Rutkowski, W. and Lipecki, T., 2023. Use of the iPhone 13 Pro LiDAR Scanner for Inspection and Measurement in the Mineshaft Sinking Process. *Remote Sensing* [online], 15(21) p. 5089. Available from: https://doi.org/10.3390/rs15215089.

Sampaio, L. F., Veiga, L. A., and Alves, S., 2023. Using Smartphones as a Measurement Platform in Geoscience Applications. *Anuário do Instituto de Geociências* [online], 46, 56179. Available from: https://revistas.ufrj.br/index.php/aigeo/article/view/56179.

Singh, S.K., Banerjee, B.P. and Raval, S., 2023. A review of laser scanning for geological and geotechnical applications in underground mining. *International Journal of Mining Science and Technology, 33(2)*, pp. 133–154.

Świerczyńska, E.J., Kurdek, D. and Jankowska, I., 2024. Accuracy of the application of mobile technologies for measurements made in headings of the Kłodawa Salt Mine. *Reports on Geodesy*, 117, pp. 55–68.

Tamimi, R. 2022. Relative Accuracy Found within Iphone Data Collection. *The International Archives of the Photogrammetry, Remote Sensing and Spatial Information Sciences,* XLIII-B2-2022, pp. 303–308.

Tavani, S., Billi, A., Corradetti, A., Mercuri, M., Bosman, A., Cuffaro, M., Seers, T. and Carminati, E., 2022. Smartphone assisted fieldwork: Towards the digital transition of geoscience fieldwork using LiDAR-equipped iPhones. *Earth-science reviews* [online], 227, p. 103969. Available from: https://doi.org/10.1016/j.earscirev.2022.103969.

Teppati Losè, L., Spreafico, A., Chiabrando, F., and Giulio Tonolo, F., 2022. Apple LiDAR Sensor for 3D Surveying: Tests and Results in the Cultural Heritage Domain. *Remote Sensing* [online], 14(17), p. 4157. Available from: https://www.mdpi.com/2072-4292/14/17/4157.

Torkan, M., Janiszewski, M., Uotinen, L., and Rinne, M., 2023. Method to obtain 3D point clouds of tunnels using smartphone LiDAR and comparison to photogrammetry. *IOP Conference Series: Earth and Environmental Science*, 1124(1), pp. 1–10.